Myosin V, Rab11, and dRip11 direct apical secretion and cellular morphogenesis in developing *Drosophila* photoreceptors

Bingbing X. Li, Akiko K. Satoh, and Donald F. Ready

Department of Biological Sciences, Purdue University, West Lafayette, IN 47907

Sensory neuron terminal differentiation tasks apical secretory transport with delivery of abundant biosynthetic traffic to the growing sensory membrane. We recently showed *Drosophila* Rab11 is essential for rhodopsin transport in developing photoreceptors and asked here if myosin V and the *Drosophila* Rab11 interacting protein, dRip11, also participate in secretory transport. Reduction of either protein impaired rhodopsin transport, stunting rhabdomere growth and promoting accumulation of cytoplasmic rhodopsin. MyoV-reduced photoreceptors also developed ectopic rhabdomeres inappropriately located in basolateral membrane, indicating a role for MyoV in photoreceptor polarity. Binary yeast two hybrids and in vitro protein–protein interaction predict a ternary complex assembled by independent dRip11 and MyoV binding to Rab11. We propose this complex delivers morphogenic secretory traffic along polarized actin filaments of the subcortical terminal web to the exocytic plasma membrane target, the rhabdomere base. A protein trio conserved across eukaryotes thus mediates normal, in vivo sensory neuron morphogenesis.

Introduction

Across eukaryotes, a protein trio comprising a Rab protein, a member of the family of small GTPases that regulate exchange between membrane compartments, a myosin motor, notably myosin V (MyoV), and a linker/adaptor protein powers organelle motility and polarized secretion (Hammer and Wu, 2002; Deneka et al., 2003; Seabra and Coudrier, 2004). For example, HeLa and MDCK cells recycle endocytosed cell surface receptors through a recycling endosome, the return leg mediated by Rab11 together with MyoV and the Rab11 adaptor/linker protein, family interacting protein 2 (FIP2) (Hales et al., 2002). *Drosophila* photoreceptors are typical polarized epithelial cells and morphogenesis of their photosensory membrane organelles, rhabdomeres, is driven by a late-pupal surge of secretory traffic that greatly expands the apical plasma membrane in a column of closely packed, rhodopsin-rich photosensitive microvilli. We recently found that Rab11 mediates membrane transport to developing rhabdomeres (Satoh et al., 2005), prompting us to ask if *Drosophila* MyoV (Bonafe and Sellers, 1998; MacIver et al., 1998) and dRip11, and *Drosophila* FIP2 (Prekeris et al., 2000) also participate in morphogenic secretory transport.

Numerous observations link MyoV to polarized membrane transport (Reck-Peterson et al., 2000). Budding yeast lacking essential MyoV, Myo2p, accumulate cytoplasmic post-Golgi secretory vesicles; secretion continues in mutants, but is not correctly targeted to the growing bud (Johnston et al., 1991). Melanocytes of mouse *dilute* mutants lacking MyoVa fail to properly localize melanosome pigment organelles to the actin-rich cell periphery; expression of a MyoVa C-terminal fragment (MyoVa-CT) that displaces endogenous MyoVa from melanosomes mimics MyoVa loss (Wu et al., 1998). Expression of MyoVa-CT similarly inhibits *Xenopus* melanosome motility (Rogers et al., 1999) and HeLa cell transferrin receptor recycling (Lapierre et al., 2001; Hales et al., 2002; Rodriguez and Cheney, 2002). Notably, in polarized MDCK cells, MyoVb-CT selectively disrupts Rab11-dependent apical, but not basolateral, membrane recycling (Lapierre et al., 2001).

Parallel loss-of-function phenotypes suggest MyoV and Rab11 cooperate in membrane transport. Loss of either activity inhibits recycling of CXCR2 chemokine and M_4 muscarinic acetylcholine receptors (Volpicelli et al., 2002; Fan et al., 2003, 2004). Similarly, MyoV or Rab11 reduction prevents biogenesis of apical cannicular membranes in polarized hepatocytes (Wakabayashi et al., 2005) and decreases glutamate receptor 1

B.X. Li and A.K. Satoh contributed equally to this paper.

Correspondence to D.F. Ready: dready@bilbo.bio.purdue.edu

Abbreviations used in this paper: FIP, family interacting protein; MyoV, myosin V; RBD, Rab11 binding domain; Rh1, rhodopsin1; RTW, rhabdomere terminal web.

The online version of this article contains supplemental material.

The Journal of Cell Biology, Vol. 177, No. 4, May 21, 2007 659-669
http://www.jcb.org/cgi/doi/10.1083/jcb.200610157

(GluR1) subunit delivery to developing synapses of hippocampal cells in culture (Lise et al., 2006).

Direct interaction between rabbit Rab11a and MyoVb is detected in yeast two-hybrid screens (Lapierre et al., 2001), and deletion of MyoVb-CT's Rab11 binding sequence neutralizes its dominant-negative impact on GluR1 delivery in hippocampal neurons, suggesting MyoVb binds Rab11 in GluR1 trafficking (Lise et al., 2006). Genetic interaction between *Saccharomyces cerevisiae* Myo2p and Sec4p mutants is consistent with direct or close cooperation (Schott et al., 1999).

In addition to MyoV, Rab11 interacts with Rab11-FIPs at a signature Rab11 binding domain (RBD) (Prekeris, 2003). Class I FIPs contain a C2 domain that targets recycling vesicles to the plasma membrane (Lindsay and McCaffrey, 2004), and truncated FIPs lacking the C2 domain inhibit receptor recycling (Cullis et al., 2002; Lindsay et al., 2002; Meyers and Prekeris, 2002; Peden et al., 2004). *Drosophila* encodes a single class I FIP, dRip11 (Prekeris et al., 2000), but its function has not been reported.

The *Drosophila* genome includes a single MyoV gene, *myoV* (*didum*) (Bonafe and Sellers, 1998; MacIver et al., 1998). *Drosophila* embryos receive substantial maternal MyoV and the protein is ubiquitously expressed throughout development, including the adult retina, where it localizes to the base of the rhabdomere (Mermall et al., 2005). Mutants lacking MyoV show strong developmental delays and substantial late larval lethality. Surprisingly, rare homozygous mutant escapers showed normal embryogenesis and cellular architecture, suggesting MyoV is dispensable for the wide range of membrane trafficking that supports normal development (Mermall et al., 2005). Actin staining of *myoV* mutant eyes showed apparently normal rhabdomeres and adult mutants were normally phototaxic, suggesting that MyoV does not play an obvious role in rhabdomere development or photoreception (Mermall et al., 2005).

In this paper, we investigate the role of MyoV and dRip11 in the polarized membrane transport that builds *Drosophila* rhabdomeres. We find both are essential. In MyoV mutants, rhodopsin 1 (Rh1) is not delivered to the growing rhabdomere, but instead accumulates in photoreceptor cytoplasm; rhodopsin-bearing vesicles, and the Rab11 and dRip11 they carry, do not approach the rhabdomere base. dRip11 loss similarly impairs secretory transport, delocalizing MyoV and Rab11 and promoting cytoplasmic Rh1. MyoV mutant photoreceptors also develop supernumerary rhabdomeres ectopically positioned within basolateral plasma membrane, suggesting MyoV-mediated transport suppresses formation of inappropriate rhabdomere primordia. *Drosophila* photoreceptors harness an evolutionarily conserved protein trio to deliver polarized apical membrane traffic in cellular morphogenesis.

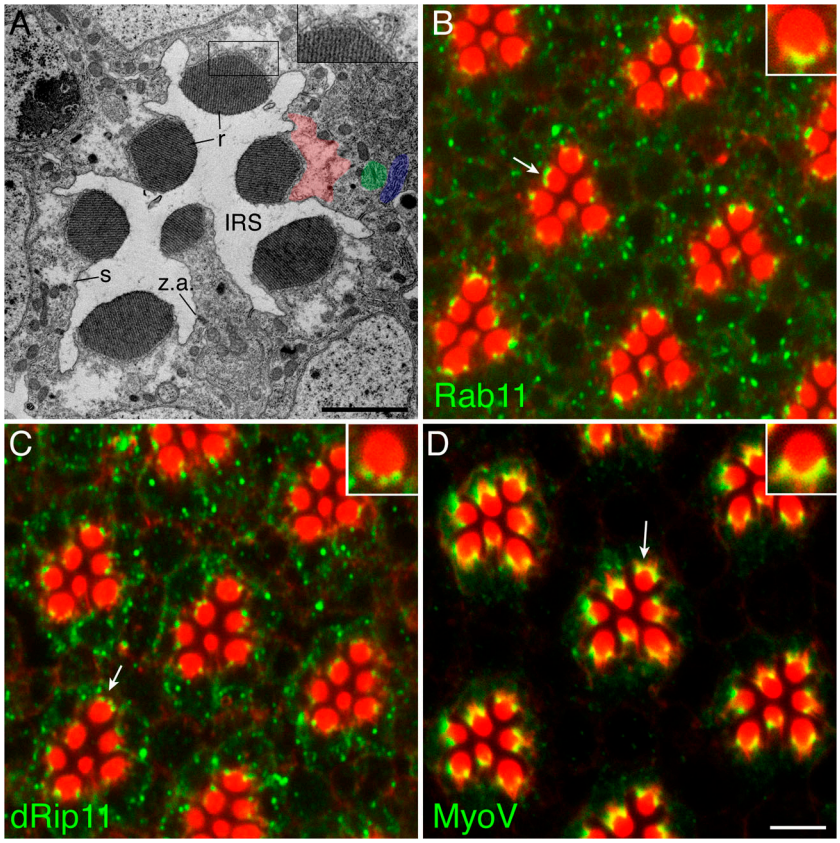

Figure 1. **Late pupal photoreceptors build rhabdomeres via targeted apical exocytosis.** (A) In a tangential thin-section electron micrograph of a single *Drosophila* unit eye or ommatidium, rhabdomeres (r) fold the expanding sensory membrane in a cylindrical stack of closely packed microvilli. Rhabdomeres constitute a central subdomain of the photoreceptor apical plasma membrane. A relatively unamplified domain, the stalk (s), surrounds rhabdomeres and anchors them to the retina's zonula adherens (z.a.) junctional network. Rhabdomere and stalk project into a trapped apical cavity, the IRS; photoreceptor basolateral membranes appose basolateral membranes of neighboring photoreceptors and surrounding pigment and cone accessory cells. Rhabdomeres grow as microvilli elongate, fed by vesicular traffic delivered to the rhabdomere base, the plasma membrane target for morphogenic secretion. The rhabdomere base presents a curving line of loops as membrane recurves to connect cytoplasmic ends of adjacent microvilli. Complex membrane profiles at the rhabdomere base are consistent with dynamic membrane traffic to and from the sensory membrane. Organelle-poor RTW cytoplasm (red highlight) extends deep into the photoreceptor; its cytoplasmic end approximates biosynthetic Golgi (green highlight) and ER (blue highlight). Multivesicular bodies package endocytosed plasma membrane. (B) Rab11 is abundant in late pupal photoreceptors. A confocal micrograph of a late pupal eye whole-mount stained for F-actin (red) and Rab11. Rab11 (green) staining is punctate through the cytoplasm with notable concentration at the rhabdomere base. Microvillar axial microfilaments show rhabdomeres bright red; wispy RTW microfilaments extend into photoreceptor cytoplasm. Inset shows higher magnification of arrowed rhabdomere. (C) dRip11 immunofluorescence resembles Rab11, with cytoplasmic puncta and localization to the rhabdomere base. (D) MyoV localizes strongly to the rhabdomere base of light-adapted late pupal photoreceptors. MyoV is prominent in the RTW and especially along the rhabdomere base. Cytoplasmic MyoV is diffuse, with occasional puncta. Bars: (A) 2 μm; (B–D) 5 μm.

Results

Rab11, dRip11, and MyoV localize to the developing rhabdomere base

Morphogenic secretory traffic targets the rhabdomere base, the plasma membrane at the cytoplasmic ends of the sensory microvilli (Fig. 1). Cytoplasm adjacent to the rhabdomere base is permeated by a dense microfilament brush, the rhabdomere terminal web (RTW), which extends from the rhabdomere base deep into photoreceptor cytoplasm (Arikawa et al., 1990; Chang and Ready, 2000). Microfilaments are poorly preserved in chemically fixed tissue, but distinct "RTW cytoplasm" is manifest as organelle-poor cytoplasm behind the rhabdomere (Fig. 1 A, red highlight). RTW cytoplasm excludes even ribosomes, whose absence contributes to the light, clear appearance of RTW cytoplasm. Biosynthetic ER (blue highlight) and Golgi (green highlight) are distributed the length of the cell, in close proximity to the RTW's cytoplasmic terminus.

The rhabdomere base differentiates in mid-pupal photoreceptors as the photoreceptor apical membrane resolves to a central Moesin-rich rhabdomere primordium surrounded by a Crumbs-rich supporting domain (Izaddoost et al., 2002; Pellikka et al., 2002; Karagiosis and Ready, 2004). Once founded, the rhabdomere base organizes the RTW and receives morphogenic traffic. The stalk accepts little traffic, focusing exocytosis to the rhabdomere. The stalk links the rhabdomere to the retina's junctional network and projects it into an apical lumen, the IRS, aligned to the eye's optical axis (Fig. 1 A).

Membrane transport in light-adapted late pupal photoreceptors is dynamic, with biosynthetic and endocytic traffic reflected in numerous, complex membrane compartments (Fig. 1 A). Post-Golgi secretory traffic is carried in tubular vesicles, approximately 100 nm across; endocytosed membrane gathers in multivesicular bodies. Complex membrane forms are common at the rhabdomere base, likely a consequence of extensive membrane fusion.

Confocal immunofluorescence localizes Rab11 to puncta throughout photoreceptor cytoplasm, with a prominent concentration at the rhabdomere base (Fig. 1 B) (Satoh et al., 2005). dRip11 immunolocalization resembled Rab11, with cytoplasmic puncta and localization at the rhabdomere base (Fig. 1 C). Note that Rab11 and dRip11 lie within RTW cytoplasm, overlapping the actin brush extending from the rhabdomere's curving base. MyoV concentrates across the rhabdomere base of late pupal photoreceptors, often appearing strongest at the sides (Fig. 1 D). Like Rab11 and dRip11, MyoV staining was strongly within RTW cytoplasm. Cytoplasmic MyoV was lightly diffuse with scattered brighter puncta. Westerns and genetic removal verified antibodies (Fig. S1, available at http://www.jcb.org/cgi/content/full/jcb.200610157/DC1).

Rab11, MyoV, and dRip11 interact in yeast-two hybrids

We used binary yeast two-hybrid assays to evaluate potential interactions among MyoV, Rab11, and dRip11. In AH109 yeast, we found strong interaction between full-length Rab11 and three truncated MyoV tail proteins; in PJ69, the shortest tail fragment tested, aa 1383–1800 did not support colony growth, while longer fragments aa 922–1800 and aa 1063–1800 did (Fig. S2 A, available at http://www.jcb.org/cgi/content/full/jcb.200610157/DC1). β-galactosidase expression in PJ69 detects Rab11 interaction for all three MyoV constructs (Fig. S2 B).

Yeast two hybrids show dRip11 binds Rab11. Rab11 bound to a longer aa 726–821, but not a shorter aa 753–806 dRip11 fragment (Fig. S2 C); both contain the RBD aa 782–802, but only closely for the shorter construct, possibly compromising efficient binding.

Binary two-hybrid growth assay detected no binding between full-length dRip11 and any of four dRip11 fragments, aa 107–832, aa 107–530, aa 513-660, and aa 513–832, and three truncated MyoV tail proteins, aa 922–1800, aa 1063–1800, and aa 1383–1800 (unpublished data).

In vitro protein–protein binding confirmed direct Rab11–MyoV interaction. Epitope-tagged, biotinylated Rab11, MyoV, and control proteins p53 and TD1 were produced using an in vitro transcription/translation system, pairwise mixed, incubated, and immunoprecipitated using epitope-specific antibodies. Myc-Rab11 specifically coimmunoprecipitated MyoV (Fig. S2 D).

Yeast two hybrids and in vitro protein interactions thus predict a ternary complex assembled by independent MyoV and dRip11 binding to Rab11.

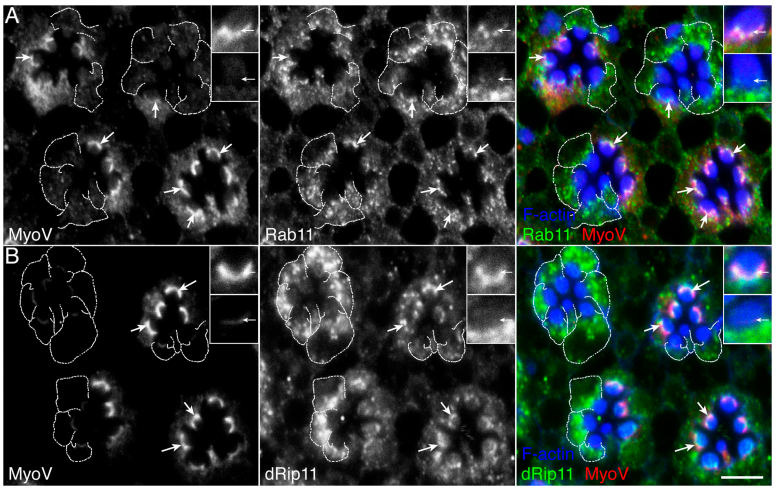

Figure 2. **MyoV reduction delocalizes Rab11 and dRip11 from the rhabdomere base.** Confocal micrographs of mosaic eyes containing a mixture of normal and *MyoV*^{Q1052st} mutant photoreceptors (dashed outlines) double immunostained for (A) MyoV (left, red) and Rab11 (middle, green), or (B) MyoV (left, red) and dRip11 (middle, green). In merged images of normal cells note MyoV, Rab11, and dRip11 colocalize at the rhabdomere base, well within RTW cytoplasm. In mutant cells, Rab11 and dRip11 appear largely excluded from the RTW and rhabdomere base. Top and bottom insets show higher magnification wild-type and *MyoV*^{Q1052s} mutant rhabdomeres. Bar, 5 μm.

MyoV reduction delocalizes Rab11 and dRip11 from the rhabdomere base

To investigate potential MyoV function, we examined Rab11 and dRip11 distribution in normal and MyoV mutant photoreceptors (Fig. 2). MyoV bright crescents marked rhabdomere bases of normal photoreceptors (Fig. 2, A and B). Rab11 (Fig. 2 A) and dRip11 (Fig. 2 B) colocalize with MyoV at the rhabdomere base, well within RTW cytoplasm, often appearing as a lumpy and interrupted crescent overlapping MyoV. In mutant photoreceptors MyoV is strongly reduced, showing virtually no cytoplasmic and weak rhabdomere base staining. Mutant photoreceptor actin cytoskeletons appear largely normal, with well-formed RTWs, suggesting cytoskeletal organization withstands strong MyoV reduction and that RTW cytoplasm is largely intact.

MyoV reduction depletes Rab11 (Fig. 2 A) and dRip11 (Fig. 2 B) from the rhabdomere base. In mutant photoreceptors, Rab11 and dRip11 are excluded from RTW cytoplasm, standing off from the rhabdomere base. They otherwise retain a generally punctate, membrane-associated appearance, suggesting Rab11 and dRip11 do not require MyoV for vesicle attachment. Although not quantitated, Rab11 and dRip11 staining often seem enhanced in mutant photoreceptors.

MyoV loss compromises Rh1 transport

Delocalization of Rab11 and dRip11 from the rhabdomere base could reflect failure of secretory vesicles to transit the RTW, so we asked if Rh1 transport was also defective in MyoV mutant photoreceptors. In normal photoreceptors, efficient transport to the growing rhabdomere keeps pace with biosynthesis and cytoplasmic Rh1 is limited to scattered puncta. Rh1 concentrates in rhabdomeres and in Rh1-positive large vesicles, multivesicular bodies containing endocytosed Rh1 (Fig. 3 A). By contrast, abundant cytoplasmic Rh1 accumulates in photoreceptors of rare homozygous $MyoV^{Q1052st}$ escapers; late pupal escaper rhabdomeres show virtually no Rh1 (Fig. 3 B), though occasional adult escaper rhabdomeres show some Rh1. In mosaic eyes containing large homozygous $MyoV^{Q1052st}$ patches (e.g., covering roughly a quarter of the eye), mutant photoreceptors likewise show cytoplasmic Rh1 and small rhabdomeres (Fig. 3 C). These rhabdomeres contain some Rh1, indicating limited transport still operates, presumably mediated by MyoV persisting after recombination renders cells genetically *MyoV* null. In smaller patches containing a handful of mutant cells, cytoplasmic Rh1 is also observed, but rhabdomeres are larger and strongly Rh1 positive (Fig. 3 D). We speculate clone size correlates roughly with MyoV reduction,

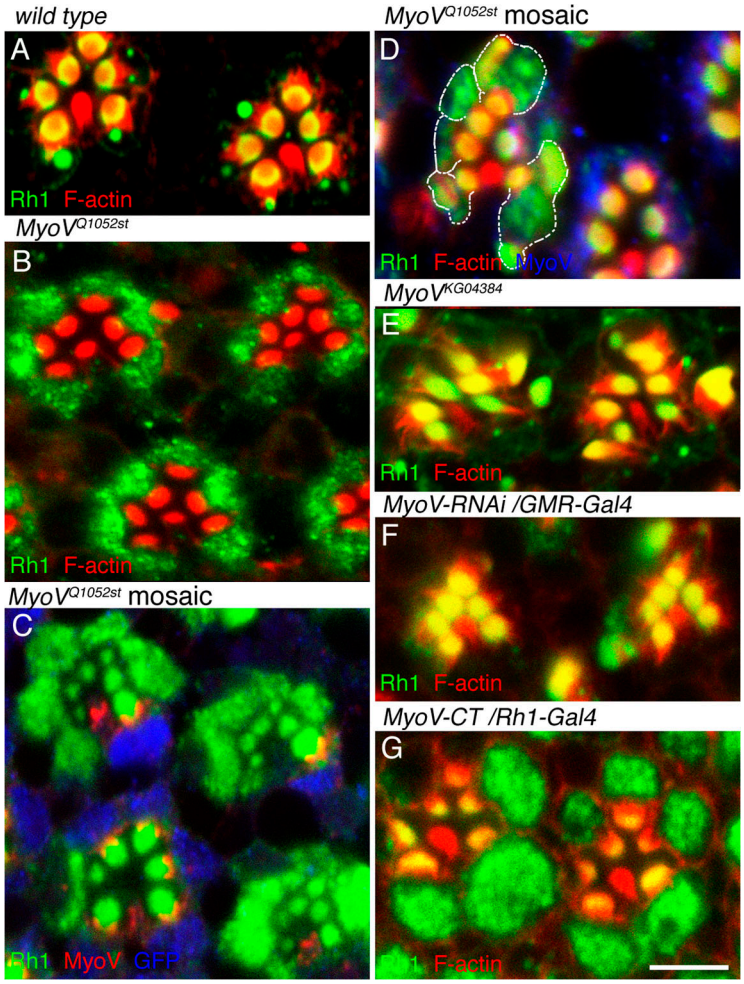

Figure 3. **Cytoplasmic rhodopsin accumulates in MyoV mutant photoreceptors.** (A) In normal photoreceptors, Rh1 concentrates in outer photoreceptor rhabdomeres; central R7 expresses a distinct rhodopsin and does not stain. Rh1-positive large vesicles are prominent in cytoplasm. (B) In a late pupal $MyoV^{Q1052st}$ homozygote escaper, Rh1 accumulates in photoreceptor cytoplasm; virtually none is detected in rhabdomeres. (C) In a large patch covering ~25% of the eye, homozygous $MyoV^{Q1052st}$ photoreceptors show cytoplasmic rhodopsin and small rhabdomeres containing modest to moderate staining. Non-mutant cells, marked by GFP (blue), show MyoV staining, large rhodopsin-positive rhabdomeres, and little cytoplasmic rhodopsin. (D) $MyoV^{Q1052st}$ mutant photoreceptors in a small mosaic eye patch, containing a handful of mutant cells (outlined), show cytoplasmic rhodopsin; rhabdomeres are large and rhodopsin immunopositive. (E) Rhabdomeres of hypomorphic $MyoV^{KG04382}$ photoreceptors are large and rhodopsin positive; little cytoplasmic rhodopsin is apparent. (F) Photoreceptors in which a MyoV-RNAi construct (nt 1501–1860) is expressed resemble $MyoV^{KG04382}$ hypomorphs, with large rhabdomeres and little cytoplasmic rhodopsin. A second construct (nt 4801–5160) gave the same phenotype (not depicted). Note ectopic rhabdomeres (see Results) in D, E, and F. (G) MyoV-CT expressed using Rh1-Gal4 during rhabdomere development causes small rhabdomeres and cytoplasmic rhodopsin. Bar, 5 μm.

with larger clones founded early in development diluting perdurant MyoV among more progeny cells and allowing for increased MyoV turnover; conversely, cells in small clones are milder hypomorphs.

MyoV^{KG04384} has a P-element insertion on first exon, 4 bp after the start codon. Consistent with a hypomorphic allele, faint but detectable MyoV is observed in Western blots of homozygous *MyoV*^{KG04384} (not depicted), although it appears absent in immunostained eyes.

In accord with Mermall et al. (2005), we observe substantial larval lethality and developmental delay in MyoV null homozygotes. Escapers are rare; 84 of 86 individually tracked homozygotes died as midsized, apparently second instar larvae over the three weeks after hatching. Overall, we find escaper nulls with a frequency of ~2%. We propose that abundant, maternally supplied MyoV is long-lived and severely reduced protein numbers can still affect membrane delivery, albeit at a reduced rate. Chance fluctuation in maternal MyoV in amount and/or distribution into cellularizing embryos may confer just enough activity to sustain development.

Little cytoplasmic Rh1 was observed in photoreceptors homozygous for hypomorphic *MyoV*^{KG04384} (Fig. 3 E), or in photoreceptors expressing MyoV-RNAi (Fig. 3 F). We also reduced MyoV activity by expressing MyoV-CT during rhabdomere morphogenesis, and this resulted in strong accumulation of cytoplasmic Rh1 and rhabdomere reduction (Fig. 3 G).

MyoV reduction produces ectopic rhabdomeres

A striking phenotype of MyoV reduction is the appearance of ectopic rhabdomeres. In addition to principal rhabdomeres of relatively normal size and shape, extending up to 80 microns in length, MyoV mutant photoreceptors often sport rhabdomere "patches", typically a few microns deep with profiles ranging from small, malformed microvillar groups to well-formed rhabdomeres as large or larger than principal rhabdomeres and inappropriately positioned in basolateral membrane (Fig. 4). Ectopic rhabdomeres are prominent in *MyoV*^{KG04384} hypomorphs (Fig. 4 A and Fig. 3 E), *MyoV*^{Q1052st} mosaic patches (Fig. 4 B and Fig. 3 D), and in eyes in which MyoV RNAi is driven using GMR-Gal4, which begins expression at the onset of photoreceptor differentiation in the retinal epithelium (Fig. 4 C and Fig. 3 F). Ectopic rhabdomeres are present, but less common, in null homozygotes (Fig. 4 D). We propose limited MyoV activity is required to fully manifest ectopic rhabdomeres.

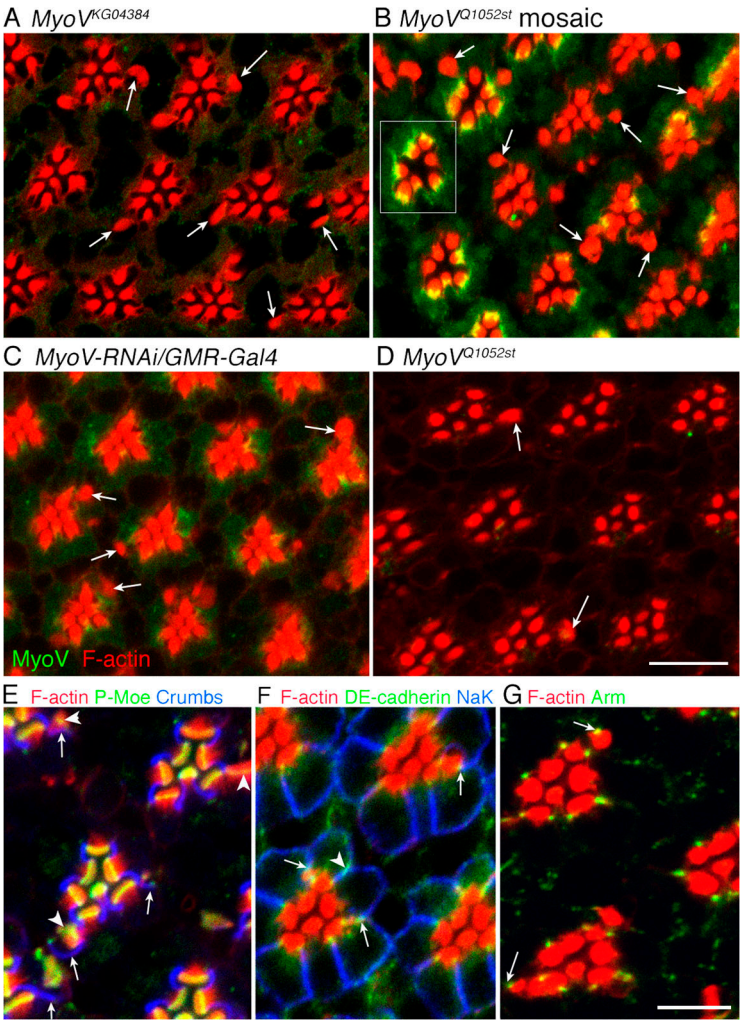

Figure 4. **MyoV reduction generates ectopic rhabdomeres.** Apart from normal principal rhabdomeres, whose overall organization is normal (boxed ommatidium in B), MyoV hypomorphic photoreceptors often sport rhabdomere "patches", microvillar fields of variable size and organization typically positioned inappropriately in basolateral membrane (arrows). Mutant photoreceptors often have one or more ectopic rhabdomeres, typically a few microns across, and a single confocal image plane may or may not cross an ectopic rhabdomere. Ectopic rhabdomeres organize RTWs and load rhodopsin (Fig. 3, D–F). Ectopic rhabdomeres are common in (A) *MyoV*^{KG04382} hypomorphs, (B) *MyoV*^{Q1052st} mosaic eyes, and (C) eyes expressing MyoV-RNAi constructs under GMR-Gal4 control. (D) Ectopic rhabdomeres are present, but less common in escaper *MyoV*^{Q1052st} homozygotes. (E–G) *MyoV*^{KG04384} mutant photoreceptors mislocalize apical proteins to ectopic rhabdomeres. (E) Like normal rhabdomeres, ectopic rhabdomere bases stain for active phospho-Moesin (arrowheads). Crumbs-immunopositive membrane (arrows) often, but not always, flanks ectopic rhabdomeres. (F) DE-cadherin normally stains junctional complexes; in homozygous *MyoV*^{KG04384} photoreceptors it is associated with aberrant junctions flanking ectopic rhabdomeres (arrows). DE-cadherin occasionally overlaps inappropriately with basolateral marker, Na^+-K^+ ATPase (arrowhead). (G) Armadillo localizes to junctions adjacent to ectopic rhabdomeres (arrows). Bars: (A–D) 10 µm; (E–G) 5 µm.

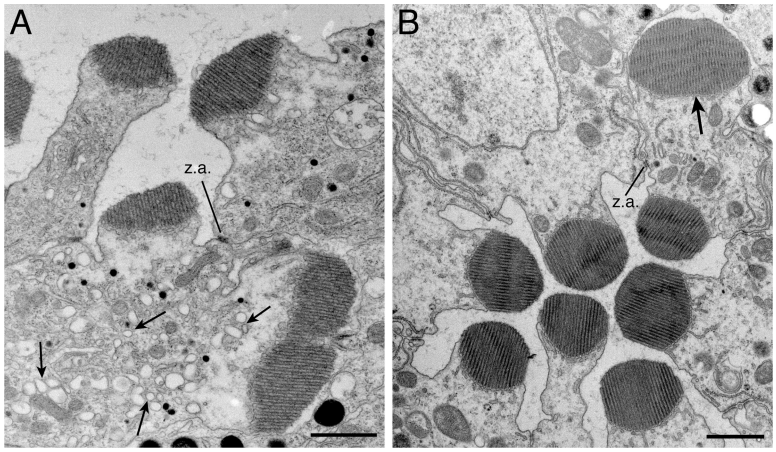

Figure 5. **MyoV mutant photoreceptors accumulate cytoplasmic vesicles.** (A) In a *MyoV*^{Q1052st} mosaic eye, photoreceptor R1 cytoplasm is filled with a profusion of large, irregular vesicles (arrows); an ectopic rhabdomere has formed on the basolateral side of the zonula adherens junctions (z.a.) that delimits the normal apical membrane. Small black spots in photoreceptors and larger spots in pigment cells are pigment granules. (B) In a *MyoV*^{KG04382} homozygote eye, photoreceptor R3 sports an ectopic rhabdomere basolateral to its z.a. junctions (arrow). Rh1 does not accumulate in *MyoV*^{KG04382} homozygote cytoplasm (Fig. 3 F), and mutant cytoplasm does not show a proliferation of vesicles. Bars, 1 μm.

MyoV mutant cells accumulate cytoplasmic vesicles

We used electron microscopy in order investigate the impact of MyoV loss in cytoplasmic organization. Abnormal vesicles crowd MyoV mutant photoreceptor cytoplasm (Fig. 5 A). These appear empty with irregular profiles typically 200–400 nm across, substantially larger than normal secretory vesicles. Whether these vesicles result from homotypic fusion of stalled and undelivered post-Golgi traffic or if MyoV shapes the morphology of post-Golgi vesicles, for example pulling buds from TGN tubules, remains to be determined.

Ultrastructurally, ectopic rhabdomere microvilli fully resemble those of normal rhabdomeres in dimension and packing; like normal rhabdomeres, a well-ordered line of membrane loops mark ectopic rhabdomere bases. Often, but not always, plasma membrane immediately adjacent to ectopic rhabdomeres has the "flattened" appearance characteristic of the stalk domain that surrounds normal rhabdomeres. Cross sections of large, well-organized ectopic rhabdomeres can rival normal rhabdomeres (Fig. 5 B).

Ectopic rhabdomeres first become apparent in mid-pupal MyoV hypomorphs with the appearance of isolated actin-rich plasma membrane patches that resemble the rhabdomere primordium of the normal rhabdomere. MyoV-CT expression at 45% pupal development using relatively brief 20-min heat shocks produces ectopic rhabdomeres (unpublished data). As true for

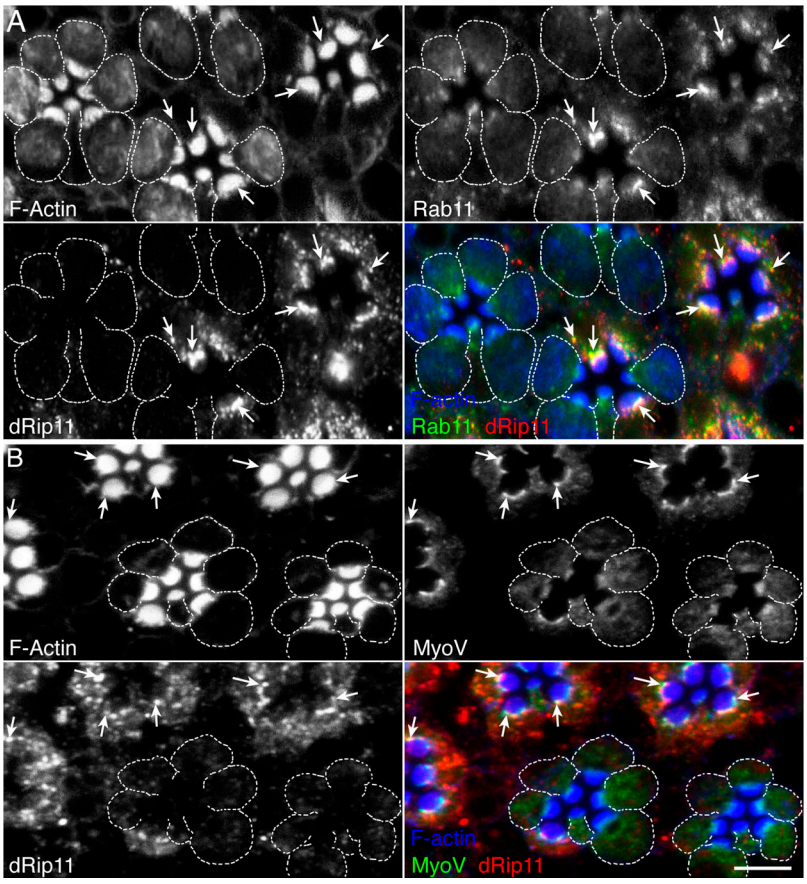

Figure 6. **dRip11 loss delocalizes Rab11 and MyoV from the rhabdomere base.** Late pupal mosaic eyes containing homozygous *dRip11*^{KG02485} patches were stained for dRip11 (red), F-actin (blue), and either (A) Rab11 (green) or (B) MyoV (green). In wild-type cells, Rab11 and dRip11 colocalize at the rhabdomere base and cytoplasmic vesicles (A, arrows). Rab11 and MyoV also colocalize at the rhabdomere base (B, arrows). Rab11 does not concentrate at the base of dRip11-reduced photoreceptors (dashed outlines). Rab11 is diffuse in mutant cytoplasm, with occasional puncta. Rhabdomeres are reduced and the actin cytoskeleton is disturbed, with diffuse cytoplasmic F-actin not observed in wild-type cells. Sharply focused MyoV immunostaining at the rhabdomere base of normal cells is reduced in dRip11-reduced cells (dashed outlines). Some MyoV overlaps the RTW at mutant rhabdomere bases. Bar, 5 μm.

normal rhabdomeres, activated Moesin defines the ectopic rhabdomere base. Ectopic rhabdomeres are often, but not always, flanked by Crb-positive stalk membrane and ectopic cell–cell junctions marked by β-catenin and E-cadherin (Fig. 4, E–G). A set of apical membrane proteins is thus mislocalized when MyoV is reduced.

dRip11 is the sole *Drosophila* class I FIP

As noted by Prekeris et al. (2000), the *Drosophila* genome contains a single class I FIP, dRip11, the product of homozygous lethal *l(1)G0003*(CG6606). Entire dRip11 aligns with human class I FIPs, Rip11, Rab11-FIP2, and RCP (Fig. S3, available at http://www.jcb.org/cgi/content/full/jcb.200610157/DC1). As true for FIPs generally, dRip11 is not significantly similar to other FIPs outside of these shared homology domains. Notably, dRip11 does not contain the NPF domains that couple Rab11-FIP2 to Reps1, an EH domain protein that promotes endocytosis (Cullis et al., 2002; Naslavsky et al., 2006). Similar to RCP, dRip11 contains two PEST domains that potentially promote rapid degradation (Marie et al., 2005). dRip11 also conserves Rab11-FIP2 Ser258, phosphorylated by MARK2 in MDCK cells, and corresponding to dRip11 S262 (Ducharme et al., 2006).

dRip11 localizes Rab11 and MyoV to the rhabdomere base

To test for dRip11 function, we made mosaic eyes containing *dRip11*^{KG02485} patches. In normal photoreceptors, Rab11 and dRip11 colocalize extensively and concentrate at the rhabdomere base and cytoplasmic vesicles (Fig. 6 A). Occasional puncta stain for only one of the proteins, suggesting they may not be obligatory partners. MyoV and dRip11 likewise colocalize at the rhabdomere base of normal cells (Fig. 6 B). Anti-dRip11 staining is strongly reduced in mutant photoreceptors. Strikingly, in dRip11-deficient cells, Rab11 and MyoV are lost from the rhabdomere base. Rhabdomeres are reduced and the actin cytoskeleton is disturbed, with diffuse cytoplasmic F-actin not observed in wild-type cells.

dRip11 is necessary for Rh1 transport

We assessed dRip11's role in Rh1 transport during development using confocal immunohistochemistry to localize Rh1 in wild-type and mutant photoreceptors. Like MyoV and Rab11 loss, dRip11 mutant photoreceptors show loss of rhabdomere Rh1 staining and cytoplasmic accumulation throughout cytoplasm (Fig. 7). Rhabdomeres are strongly reduced in dRip11 mutant cells and photoreceptor cytoplasm fills with a profusion of abnormal vesicles. As Rab11-FIP C-terminal is dominant-negative for normal membrane traffic in mammalian cells in culture (Hales et al., 2002; Lindsay and McCaffrey, 2004), we asked if expression of dRab11-CT also impairs Rh1 transport in developing photoreceptors. Late pupal expression of a dRab11-CT (700–821) GFP fusion protein, dRip11-CT-GFP, delocalized Rab11 (Fig. S4, available at http://www.jcb.org/cgi/content/full/jcb.200610157/DC1). dRip11-CT-GFP contains the RBD, and our two-hybrid results showed dRab11-CT (726–821) interacts with Rab11. Diffuse but occasionally still punctate Rab11 colocalizes with dRip11-CT-GFP (Fig. S4 A, arrow). Rh1 accumulates in the cytoplasm and there is no Rh1 staining in rhabdomeres. Cytoplasmic F-actin accumulation is also seen. Electron micrographs showed massive accumulation of abnormal vesicles (unpublished data). dRip11-CT-GFP overexpression strongly phenocopies *dRip11*^{KG02485} patches of mosaic eyes.

Discussion

Drosophila photoreceptors, like many polarized epithelial cells, greatly amplify their apical membranes during terminal differentiation via targeted membrane delivery. Here we show that

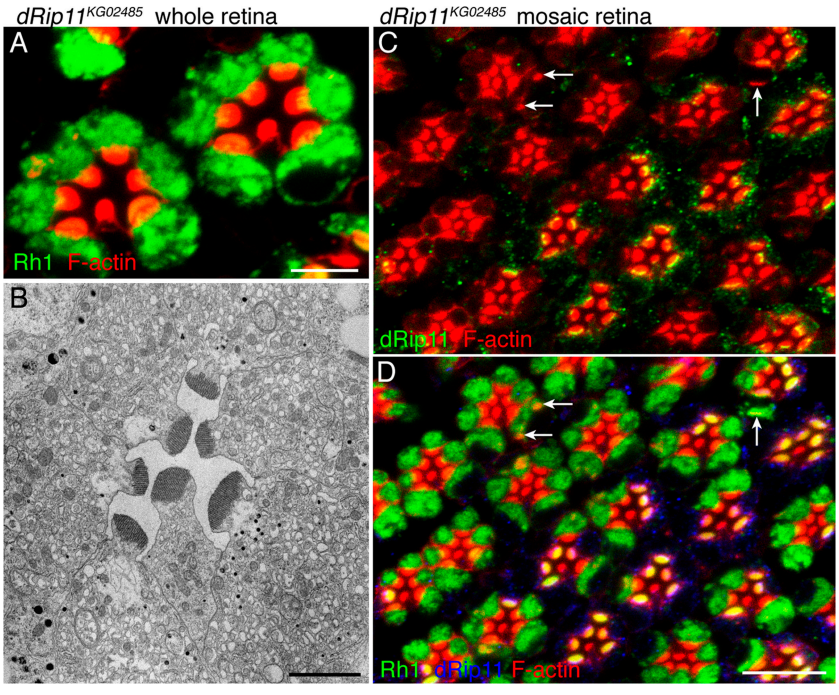

Figure 7. **Rh1 transport requires dRip11.** (A) Homozygous *dRip11*^{KG02485} late pupal photoreceptors accumulate abundant cytoplasmic rhodopsin (green). (B) Electron micrographs show *dRip11*^{KG02485} mutant photoreceptor cytoplasm fills with vesicles, not seen in normal photoreceptors. (C) In *dRip11*^{KG02485} mosaic eyes, mutant photoreceptors form ectopic rhabdomeres (arrows); some ectopic rhabdomeres appear as thin patches, suggesting little microvillar growth. (D) In a *dRip11*^{KG02485} mosaic eye, photoreceptors lacking dRip11 (blue) cells show abundant cytoplasmic, but little rhabdomeric rhodopsin (green). Bars: (A) 5 μm; (B) 2 μm; (C and D) 10 μm.

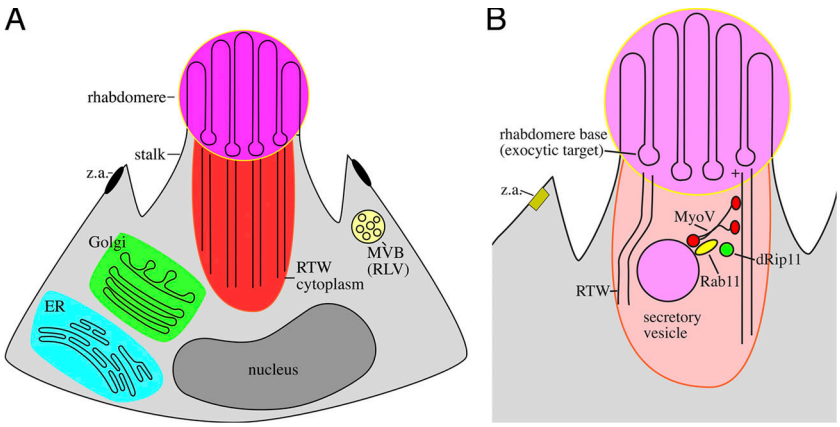

Figure 8. **A model of photoreceptor cytoplasm and apical transport.** (A) In cross section, fly photoreceptors are elongated wedge-shaped cells, with apical surfaces facing a trapped lumen. The long axis of this cell would project approximately 50 rhabdomere diameters into the plane. The RTW and its exclusionary cytoplasm emanate from the rhabdomere base. Biosynthetic ER and Golgi are distributed the length of the photoreceptor in proximity to RTW cytoplasmic ends. Endocytosed membrane containing Rh1 transits the multivesicular body. (B) Secretory vesicles are pulled through RTW cytoplasm by a MyoV–Rab11–dRip11 complex to the exocytic plasma membrane target, the rhabdomere base.

a protein trio (Rab11, dRip11, and MyoV) mediates this morphogenic secretory traffic. MyoV normally concentrates at the base and its loss causes three notable phenotypes of compromised apical transport: Rab11 and dRip11 delocalize from the base, Rh1 accumulates in photoreceptor cytoplasm, and ectopic rhabdomeres are formed. dRip11, the sole *Drosophila* class I Rab-FIP (Prekeris, 2003), is also required for normal Rh1 transport; its loss delocalizes Rab11 and MyoV. Together with our previous demonstration that Rab11 is essential for photoreceptor secretory traffic (Satoh et al., 2005), we propose MyoV pulls post-Golgi secretory vesicles, marked for rhabdomere delivery by Rab11 and dRip11, through an exclusionary subcortical cytoskeletal web along polarized microfilaments leading directly to the exocytic targeting patch at the rhabdomere base (Fig. 8).

The RTW's role as both a barrier and a carrier for morphogenic traffic is an instance of a general theme of a dynamic regulatory role of the subcortical cytoskeleton in secretion (Burgoyne and Morgan, 2003; Giner et al., 2005; Scalettar, 2006). Myosin S1 decoration shows RTW filaments are oriented with plus-ends at the membrane, a correct orientation for MyoV-based secretory transport (Arikawa et al., 1990), and disruption of the actin cytoskeleton prevents the morphogenic traffic that rebuilds crab rhabdomeres at dusk (Arikawa et al., 1987; Matsushita and Arikawa, 1996). The RTW's strong polarization and anchorage to a secretory targeting patch resembles the polarized actin cables that mediate budding yeast secretory traffic (Pruyne et al., 2004).

Absorptive and secretory epithelial cell specialists often regulate apical membrane activity by dynamic, Rab11-dependent exchange of plasma membrane with recycling endosomes. For example, gastric parietal cells meet demand for additional acid secretion by Rab11-, Rab11-FIP2-, and MyoV-dependent delivery of additional H^+/K^+ ATPase pumps to the cell surface from a recycling endosome (Duman et al., 1999; Hales et al., 2001; Lapierre et al., 2001). Like GPCRs generally, *Drosophila* Rh1 is endocytosed upon stimulation but appears to be degraded rather than recycled back to the rhabdomere (Eguchi and Waterman, 1967; Williams, 1982; Satoh et al., 2005). *Drosophila* photoreceptor Rab11-dependent transport appears to be principally devoted to delivery of newly synthesized cargo from the TGN to the plasma membrane, a conserved Rab11 activity (Chen et al., 1998) now seen to further parallel recycling transport. Ectopic rhabdomeres in hypomorphs suggest MyoV normally suppresses the establishment of inappropriate rhabdomere primordia; oncefounded ectopic rhabdomeres develop in concert with principal rhabdomeres, presumably drawing from the same secretory traffic. We speculate MyoV normally drives traffic to the differentiating rhabdomere primordium and that positive feedback driven by the incorporation of morphogenic determinants, perhaps proteins that anchor and promote RTW development, gives the original, "true" apical membrane an overwhelming growth advantage, starving weak, inappropriate sites. MyoV reduction might diminish this advantage, allowing ectopic foci to capture sufficient morphogenic traffic to assemble a rhabdomere patch.

Our observation here that MyoV is required for normal rhabdomere development differs from Mermall and colleague's report of normal rhabdomeres in $MyoV^{Q1052st}$ mutant eyes (Mermall et al., 2005). However, long ribbons of the principal rhabdomeres dominate phalloidin-stained longitudinal sections, and ectopic rhabdomeres, often patches a few microns across, are not prominent. Mermall et al.'s supplementary Fig. 1 L, a tangential section, shows actin-bright profiles apart from the principal rhabdomeres—potentially ectopic rhabdomeres. Massive biosynthetic traffic in late pupal photoreceptors sensitizes cells to compromise of efficient, accurate transport and accumulation of cytoplasmic Rh1 reflects an inability of transport to keep pace with biosynthesis.

dRip11 loss inhibits secretory transport and misolcalizes Rab11 and MyoV. We suggest dRip11 couples two broad streams of membrane transport, Rab11- and MyoV-dependent activities, to drive morphogenic secretory traffic. Results here are consistent with previously demonstrated roles for FIPs as contributors to membrane targeting (Meyers and Prekeris, 2002; Lindsay and McCaffrey, 2004), and as scaffolds for the growing Rab11 effector ensemble (Pooley et al., 2006). Similar to chromaffin cells, where MyoV only partially overlaps with secretory vesicles (Rose et al., 2003), MyoV and Rab11 only partially overlap in developing photoreceptors, and it is likely MyoV transports multiple and changing cargoes.

Rab11 participates in both constitutive and Ca^{2+}-regulated secretion (Khvotchev et al., 2003), and both cargo binding and Ca^{2+} regulate MyoV activity (Krementsov et al., 2004; Li et al., 2005; Thirumurugan et al., 2006). Rhabdomere morphogenesis

utilizes constitutive exocytosis, with substantial rhabdomere growth before Rh1 expression and photoresponse Ca^{2+} influx. Rhabdomeres likewise develop normally in the dark, indicating light-dependent Ca^{2+} elevation is not required for MyoV morphogenic transport. We propose dRip11, in proximity to MyoV via their mutual binding to Rab11 on post-Golgi secretory vesicles, interprets or conveys non-Ca^{2+}-stimulated MyoV activation, promoting developmental MyoV secretory transport.

Materials and methods

Fly stocks

Flies were reared at 20°C, 12 h light/12 h dark, on standard cornmeal agar food. White-eye flies (w^{1118}) were used as wild type.

Two MyoV null lines, *MyoV* ^{Q1052st}, predicted to introduce a nonsense mutation at residue Gln1052, and *del 28* (*dpa*; Δ28)), a deletion mutation removing *5′ myosin V* and adjacent *dpa*, with *dpa* transgenically restored, were provided by the Cooley and Mooseker labs (Mermall et al., 2005). To generate mosaic eyes *MyV* ^{Q1052st} was recombined onto FRT42B. *MyoV* ^{Q1052st} *FRT42B/Sm6TM6B* virgins were crossed to *eyFLP; FRT42B or eyFLP; FRT42B Ubi-GFP* to generate retinal clonal patches.

A transposon allele, *MyoV*^{KG04384} balanced over CyO, was obtained from the Bloomington Stock Center (#14094; Bloomington, IN). No homozygous animals were recovered in the original stock. However, upon outcrossing to w^{1118} or recombination onto FRT42D, homozygous mutant animals survived, suggesting the original chromosome contains a second site lethal(s).

A transposon allele, *dRip11*^{KG02485} balanced over *FM7c*, was obtained from the Bloomington Stock Center (#13742), and *FRT19A* was combined. *dRip11*^{KG02485} has a P-element insertion 83 bp upstream from the start codon. Males of the genotype *y w eyFLP, FRT19A* (B-# 5579) were crossed to females of the genotype *y w dRip11* ^{KG02485}*, FRT19A/FM7* virgins to generate mitotic clones. To generate whole dRip11 reduced eyes, we homozygosed *dRip11* ^{KG02485} in the eye using the EGUF method (Stowers and Schwarz, 1999). Males of the genotype *y w GMR-hid FRT19A; GAL4-ey* were crossed to virgin *y w dRip11*^{KG02485}*, FRT19A / FM7*.

Construction of transgenic flies expressing MyoV inverted repeats, dominant-negative GFP-MyoV-CT and dominant-negative GFP-dRip11-CT

Each of two constructs encoding MyoV (nt 1501–1860 and 4801–5160) inverted repeats (IR-MyoV) was inserted into pWIZ vector (Lee and Carthew, 2003) to produce hairpin RNAs under UAS control. As MyoV CT is dominant-negative for membrane transport, we inserted MyoV CT (aa 768–1800) into pUAST-GFP vector, permitting UAS expression. As overexpression of a Rab11-FIP C-terminal fragment is dominant-negative in mammalian cells, dRip11 C-terminal (aa 700–832) was inserted into pUAST-GFP vector. These constructs were transformed into *Drosophila* and insertion strains containing a single copy of each transgene were generated by standard methods.

Generation of anti-*Drosophila* MyoV and dRip11 antibody

Rabbit affinity-purified anti-MyoV polyclonal rabbit antibody was generated against a unique MyoV tail domain peptide (aa 1783–1800: EDIELPSHLNLDEFLTKI) (Bethyl Laboratories). 6xHis-dRip11 C-terminal 133-aa (700–832) fusion protein was expressed in *Eschericia coli* cells, purified on polyhistidine affinity resin (QIAGEN). Rabbit affinity-purified anti-dRip11 antibody was raised against this fusion protein (Bethyl Laboratories).

Yeast two-hybrid analysis

S. cerevisiae strains AH109 (CLONTECH Laboratories, Inc.) and PJ69 (James et al., 1996) were co-transformed with the indicated constructs. Transformation and cell growth were done according to Matchmaker two-hybrid protocols (BD Biosciences).

Two candidate RBD dRip11 constructs, aa 726–821 and aa 753–806, were fused to the Gal4 binding domain (pGBT9.m) and Rab11 was fused to the Gal4 activation domain (pGAD.GH). MyoV truncation mutant proteins including aa 922–1800, aa 1063–1800, and aa 1383–1800 were inserted into pGADT7, and Rab11 was cloned into pGBKT7. Different dRip11 fragments, including aa 107–832, aa 107–530, aa 513–660, and aa 513–832, were inserted into pGBKT7. Standard filter-lift assays were used to assay β-galactosidase expression in PJ69 co-transformants.

In vitro MyoV–Rab11 Interaction

MyoV–Rab11 protein interaction was assayed via coimmunoprecipitation using a Matchmaker Co-IP kit (CLONTECH Laboratories, Inc.). Biotinylated HA-tagged MyoV (aa 1063–1800) and c-Myc–tagged Rab11 were produced from pGADT7-MyoV (aa 1063–180) and pGBKT7-Rab11 (full length), respectively, using a T_NT T7 Quick Coupled Transcription/Translation System (Promega) and biotinylated lysine (Promega Transcend tRNA) as directed by the manufacturer. pGBKT7-53 and pGADT7-T (CLONTECH Laboratories, Inc.) encoding murine p53 and simian virus large T antigen, respectively, were similarly produced as controls. Products were pairwise mixed with final concentrations of 200 μM GTP-γ-S, 4 mM Mg^{2+} and 1X protease inhibitor (Pierce Chemical Co.), which are present in the subsequent steps. After 1 or 4 h incubation at room temperature (RT), 10 μl anti-Myc was added for an additional 1 h at RT. Protein A–Sepahrose (3 μl) was then added to each sample. After incubation for an additional 1 h at RT, samples were centrifuged and washed four times with Wash Buffer 1 and two times with Wash Buffer 2 (both buffers from CLONTECH Laboratories, Inc.) at 4°C. Synthesized protein, unbound protein, and immunoprecipitated protein were analyzed on 12.5% SDS-PAGE gel followed by Western Blot using HRP-conjugated streptavidin (Kirkegaard & Perry Laboratories) detected using ECL detection reagents (GE Healthcare).

Immunobloting

Fly heads were dissected and immersed in T-Per tissue protein extraction reagent (Pierce Chemical Co.) with additional 8 M urea. After homogenizing fly heads, SDS-PAGE loading buffer was immediately added into the lysates, boiled for 5 min, and then centrifuged at 164,000 *g*. The supernatant was separated on 7.5% gel and transferred to PVDF membrane (Millipore), which was then probed with rabbit anti-Myo V (1:10,000), rat anti-Myo V (1:10,000), or anti-dRip11 (1:10,000). Equivalent protein loading for each sample was verified by probing the membrane with mouse anti-actin (1:10,000), a gift from Dr. J. Lessard (Cincinnati Children's Hospital Medical Center, Cincinnati, OH).

Immunohistochemistry

Fixation and staining methods are described in Satoh et al. (2005). Primary antisera were: mouse anti-Rab11(1:250; Satoh et al., 2005), rabbit anti-Rh1 (1:1,000; Satoh et al., 2005), anti-Rh1 (4C5) mouse monoclonal (DSHB), chicken anti-GFP (1:2,000; Chemicon), rabbit anti-MyoV (1:1,000; this paper), rat anti-MyoV (1:1,000; Mermall et al., 2005) and dRip11 (1:1,000; this paper). Secondary antibodies were anti–mouse, –rabbit and/or –chicken labeled with Alexa488, -568, -647 (1:300; Molecular Probes), Cy2 (1:300; GE Healthcare), or biotin-conjugated anti–rabbit (1:150), followed by streptavidin labeled with Alexa488, -647, or Texas red (1:2,000). Samples were mounted in glycerol/PBS with 1% *N*-propyl gallate to reduce fading and imaged at room temperature using a confocal microscope (MRC1024; Bio-Rad Laboratories) (Nikon 60×, 1.4 NA lens) using LaserSharp software (Bio-Rad Laboratories). To minimize bleed-through, each signal in double- or triple-stained samples was imaged separately using a single line and then merged. Acquired images were processed by ImageJ (National Institutes of Health, Bethesda, MD) and/or Photoshop7. Image processing was fully compliant with guidelines for proper digital image handling (Rossner and Yamada, 2004).

Electron microscopy

Conventional electron microscopic methods were as described in Satoh et al. (1997, 2005). Samples were observed on an electron microscope (model 300; Philips).

Online supplemental material

Fig. S1 shows verification of MyoV and dRip11 antibodies. Fig. S2 shows that Rab11 interacts with MyoV and dRip11. Fig. S3 shows Clustal alignment of dRip11, human Rab11-FIP2, human Rip11, and human RCP. Fig. S4 shows overexpression of dRip11 C-terminal phenocopies *dRip11*^{KG02485}. Online supplemental material is available at http://www.jcb.org/cgi/content/full/jcb.200610157/DC1.

We are indebted to Drs. L. Cooley and M. Mooseker for MyoV stocks and rat anti-MyoV antibody. Drs. C. Aguilar and D. Zhou provided reagents and advice for yeast two-hybrid analysis. Ms. K. O'Shaughnessey ably assisted MyoV mutant survival analysis.

This work was supported by National Institutes of Health grant EY10306.

Submitted: 31 October 2006
Accepted: 23 April 2007

References

Arikawa, K., K. Kawamata, T. Suzuki, and E. Eguchi. 1987. Daily changes of structure, function and rhodopsin content in the compound eye of the crab *Hemigrapsus sanguineus*. *J. Comp. Physiol. [A].* 161:161–174.

Arikawa, K., J.L. Hicks, and D.S. Williams. 1990. Identification of actin filaments in the rhabdomeral microvilli of *Drosophila* photoreceptors. *J. Cell Biol.* 110:1993–1998.

Bonafe, N., and J.R. Sellers. 1998. Molecular characterization of myosin V from *Drosophila melanogaster*. *J. Muscle Res. Cell Motil.* 19:129–141.

Burgoyne, R.D., and A. Morgan. 2003. Secretory granule exocytosis. *Physiol. Rev.* 83:581–632.

Chang, H.Y., and D.F. Ready. 2000. Rescue of photoreceptor degeneration in rhodopsin-null *Drosophila* mutants by activated Rac1. *Science.* 290:1978–1980.

Chen, W., Y. Feng, D. Chen, and A. Wandinger-Ness. 1998. Rab11 is required for trans-Golgi network-to-plasma membrane transport and a preferential target for GDP dissociation inhibitor. *Mol. Biol. Cell.* 9:3241–3257.

Cullis, D.N., B. Philip, J.D. Baleja, and L.A. Feig. 2002. Rab11-FIP2, an adaptor protein connecting cellular components involved in internalization and recycling of epidermal growth factor receptors. *J. Biol. Chem.* 277:49158–49166.

Deneka, M., M. Neeft, and P. van der Sluijs. 2003. Regulation of membrane transport by rab GTPases. *Crit. Rev. Biochem. Mol. Biol.* 38:121–142.

Ducharme, N.A., C.M. Hales, L.A. Lapierre, A.J.L. Ham, A. Oztan, G. Apodaca, and J.R. Goldenring. 2006. MARK2/EMMK1/Par-1B alpha phosphorylation of Rab11-family interacting protein 2 is necessary for the timely establishment of polarity in Madin-Darby canine kidney cells. *Mol. Biol. Cell.* 17:3625–3637.

Duman, J.G., K. Tyagarajan, M.S. Kolsi, H.P. Moore, and J.G. Forte. 1999. Expression of rab11a N124I in gastric parietal cells inhibits stimulatory recruitment of the H+-K+-ATPase. *Am. J. Physiol.* 277:C361–C372.

Eguchi, E., and T.H. Waterman. 1967. Changes in retinal fine structure induced in crab *Libinia* by light and dark adaptation. *Z. Zellforsch. Mikrosk. Anat.* 79:209–229.

Fan, G.H., L.A. Lapierre, J.R. Goldenring, and A. Richmond. 2003. Differential regulation of CXCR2 trafficking by Rab GTPases. *Blood.* 101:2115–2124.

Fan, G.H., L.A. Lapierre, J.R. Goldenring, J.Q. Sai, and A. Richmond. 2004. Rab11-family interacting protein 2 and myosin Vb are required for CXCR2 recycling and receptor-mediated chemotaxis. *Mol. Biol. Cell.* 15:2456–2469.

Giner, D., P. Neco, M.D. Frances, I. Lopez, S. Viniegra, and L.M. Gutierrez. 2005. Real-time dynamics of the F-actin cytoskeleton during secretion from chromaffin cells. *J. Cell Sci.* 118:2871–2880.

Hales, C.M., R. Griner, K.C. Hobdy-Henderson, M.C. Dorn, D. Hardy, R. Kumar, J. Navarre, E.K.L. Chan, L.A. Lapierre, and J.R. Goldenring. 2001. Identification and characterization of a family of Rab11-interacting proteins. *J. Biol. Chem.* 276:39067–39075.

Hales, C.M., J.P. Vaerman, and J.R. Goldenring. 2002. Rab11 family interacting protein 2 associates with myosin Vb and regulates plasma membrane recycling. *J. Biol. Chem.* 277:50415–50421.

Hammer, J.A., and X.F.S. Wu. 2002. Rabs grab motors: defining the connections between Rab GTPases and motor proteins. *Curr. Opin. Cell Biol.* 14:69–75.

Izaddoost, S., S.C. Nam, M.A. Bhat, H.J. Bellen, and K.W. Choi. 2002. *Drosophila* Crumbs is a positional cue in photoreceptor adherens junctions and rhabdomeres. *Nature.* 416:178–182.

James, P., J. Halladay, and E.A. Craig. 1996. Genomic libraries and a host strain designed for highly efficient two-hybrid selection in yeast. *Genetics.* 144:1425–1436.

Johnston, G.C., J.A. Prendergast, and R.A. Singer. 1991. The *Saccharomyces cerevisiae MYO2* gene encodes an essential myosin for vectorial transport of vesicles. *J. Cell Biol.* 113:539–551.

Karagiosis, S.A., and D.F. Ready. 2004. Moesin contributes an essential structural role in *Drosophila* photoreceptor morphogenesis. *Development.* 131:725–732.

Khvotchev, M.V., M.D. Ren, S. Takamori, R. Jahn, and T.C. Sudhof. 2003. Divergent functions of neuronal Rab11b in Ca2+-regulated versus constitutive exocytosis. *J. Neurosci.* 23:10531–10539.

Krementsov, D.N., E.B. Krementsova, and K.M. Trybus. 2004. Myosin V: regulation by calcium, calmodulin, and the tail domain. *J. Cell Biol.* 164:877–886.

Lapierre, L.A., R. Kumar, C.M. Hales, J. Navarre, S.G. Bhartur, J.O. Burnette, D.W. Provance Jr., J.A. Mercer, M. Bahler, and J.R. Goldenring. 2001. Myosin vb is associated with plasma membrane recycling systems. *Mol. Biol. Cell.* 12:1843–1857.

Lee, Y.S., and R.W. Carthew. 2003. Making a better RNAi vector for *Drosophila*: use of intron spacers. *Methods.* 30:322–329.

Li, X.D., R. Ikebe, and M. Ikebe. 2005. Activation of myosin Va function by melanophilin, a specific docking partner of myosin Va. *J. Biol. Chem.* 280:17815–17822.

Lindsay, A.J., and M.W. McCaffrey. 2004. The C2 domains of the class I Rab11 family of interacting proteins target recycling vesicles to the plasma membrane. *J. Cell Sci.* 117:4365–4375.

Lindsay, A.J., A.G. Hendrick, G. Cantalupo, F. Senic-Matuglia, B. Goud, C. Bucci, and M.W. McCaffrey. 2002. Rab coupling protein (RCP), a novel Rab4 and Rab11 effector protein. *J. Biol. Chem.* 277:12190–12199.

Lise, M.F., T.P. Wong, A. Trinh, R.M. Hines, L.D. Liu, R.J. Kang, D.J. Hines, J. Lu, J.R. Goldenring, Y.T. Wang, and A. El-Husseini. 2006. Involvement of myosin Vb in glutamate receptor trafficking. *J. Biol. Chem.* 281:3669–3678.

MacIver, B., A. McCormack, R. Slee, and M. Bownes. 1998. Identification of an essential gene encoding a class-V unconventional myosin in *Drosophila melanogaster*. *Eur. J. Biochem.* 257:529–537.

Marie, N., A.J. Lindsay, and M.W. McCaffrey. 2005. Rab coupling protein is selectively degraded by calpain in a Ca2+-dependent manner. *Biochem. J.* 389:223–231.

Matsushita, A., and K. Arikawa. 1996. Disruption of actin filament organization by cytochalasin D inhibits rhabdom synthesis in the compound eye of the crab *Hemigrapsus sanguineus*. *Cell Tissue Res.* 286:167–174.

Mermall, V., N. Bonafe, L. Jones, J.R. Sellers, L. Cooley, and M.S. Mooseker. 2005. *Drosophila* myosin V is required for larval development and spermatid individualization. *Dev. Biol.* 286:238–255.

Meyers, J.M., and R. Prekeris. 2002. Formation of mutually exclusive Rab11 complexes with members of the family of Rab11-interacting proteins regulates Rab11 endocytic targeting and function. *J. Biol. Chem.* 277:49003–49010.

Naslavsky, N., J. Rahajeng, M. Sharma, M. Jovic, and S. Caplan. 2006. Interactions between EHD proteins and Rab11-FIP2: A role for EHD3 in early endosomal transport. *Mol. Biol. Cell.* 17:163–177.

Peden, A.A., E. Schonteich, J. Chun, J.R. Junutula, R.H. Scheller, and R. Prekeris. 2004. The RCP-Rab11 complex regulates endocytic protein sorting. *Mol. Biol. Cell.* 15:3530–3541.

Pellikka, M., G. Tanentzapf, M. Pinto, C. Smith, C.J. McGlade, D.F. Ready, and U. Tepass. 2002. Crumbs, the *Drosophila* homologue of human CRB1/RP12, is essential for photoreceptor morphogenesis. *Nature.* 416:143–149.

Pooley, R.D., S. Reddy, V. Soukoulis, J.T. Roland, J.R. Goldenring, and D.M. Bader. 2006. CytLEK1 is a regulator of plasma membrane recycling through its interaction with SNAP-25. *Mol. Biol. Cell.* 17:3176–3186.

Prekeris, R. 2003. Rabs, Rips, FIPs, and endocytic membrane traffic. *Scientific World Journal.* 3:870–880.

Prekeris, R., J. Klumperman, and R.H. Scheller. 2000. A Rab11/Rip11 protein complex regulates apical membrane trafficking via recycling endosomes. *Mol. Cell.* 6:1437–1448.

Pruyne, D., A. Legesse-Miller, L.N. Gao, Y.Q. Dong, and A. Bretscher. 2004. Mechanisms of polarized growth and organelle segregation in yeast. *Annu. Rev. Cell Dev. Biol.* 20:559–591.

Reck-Peterson, S.L., D.W. Provance, M.S. Mooseker, and J.A. Mercer. 2000. Class V myosins. *Biochim. Biophys. Acta.* 1496:36–51.

Rodriguez, O.C., and R.E. Cheney. 2002. Human myosin-Vc is a novel class V myosin expressed in epithelial cells. *J. Cell Sci.* 115:991–1004.

Rogers, S.L., R.L. Karcher, J.T. Roland, A.A. Minin, W. Steffen, and V.I. Gelfand. 1999. Regulation of melanosome movement in the cell cycle by reversible association with myosin V. *J. Cell Biol.* 146:1265–1275.

Rose, S.D., T. Lejen, L. Casaletti, R.E. Larson, T.D. Pene, and J.M. Trifaro. 2003. Myosins II and V in chromaffin cells: myosin V is a chromaffin vesicle molecular motor involved in secretion. *J. Neurochem.* 85:287–298.

Rossner, M., and K.M. Yamada. 2004. What's in a picture? The temptation of image manipulation. *J. Cell Biol.* 166:11–15.

Satoh, A., F. Tokunaga, S. Kawamura, and K. Ozaki. 1997. In situ inhibition of vesicle transport and protein processing in the dominant negative Rab1 mutant of *Drosophila*. *J. Cell Sci.* 110:2943–2953.

Satoh, A.K., J.E. O'Tousa, K. Ozaki, and D.F. Ready. 2005. Rab11 mediates post-Golgi trafficking of rhodopsin to the photosensitive apical membrane of *Drosophila* photoreceptors. *Development.* 132:1487–1497.

Scalettar, B.A. 2006. How neurosecretory vesicles release their cargo. *Neuroscientist.* 12:164–176.

Schott, D., J. Ho, D. Pruyne, and A. Bretscher. 1999. The COOH-terminal domain of Myo2p, a yeast myosin V, has a direct role in secretory vesicle targeting. *J. Cell Biol.* 147:791–807.

Seabra, M.C., and E. Coudrier. 2004. Rab GTPases and myosin motors in organelle motility. *Traffic.* 5:393–399.

Stowers, R.S., and T.L. Schwarz. 1999. A genetic method for generating *Drosophila* eyes composed exclusively of mitotic clones of a single genotype. *Genetics.* 152:1631–1639.

Thirumurugan, K., T. Sakamoto, J.A. Hammer, J.R. Sellers, and P.J. Knight. 2006. The cargo-binding domain regulates structure and activity of myosin 5. *Nature.* 442:212–215.

Volpicelli, L.A., J.J. Lah, G.F. Fang, J.R. Goldenring, and A.I. Levey. 2002. Rab11a and myosin Vb regulate recycling of the M-4 muscarinic acetylcholine receptor. *J. Neurosci.* 22:9776–9784.

Wakabayashi, Y., P. Dutt, J. Lippincott-Schwartz, and I.M. Arias. 2005. Rab11a and myosin Vb are required for bile canalicular formation in WIF-B9 cells. *Proc. Natl. Acad. Sci. USA.* 102:15087–15092.

Williams, D.S. 1982. Rhabdom size and photoreceptor membrane turnover in a muscoid fly. *Cell Tissue Res.* 226:629–639.

Wu, X., B. Bowers, K. Rao, Q. Wei, and J.A. Hammer. 1998. Visualization of melanosome dynamics within wild-type and dilute melanocytes suggests a paradigm for myosin V function in vivo. *J. Cell Biol.* 143:1899–1918.